Mathematical Modeling of Zig-Zag Traveling-Wave Electro-Osmotic Micropumps

J. Hrdlička*, P. Červenka, M. Přibyl, and D. Šnita
Dept. of Chemical Engineering, Institute of Chemical Technology Prague
*Corresponding author: ICT Prague, Technická 5, 166 28 Praha 6, jiri.hrdlicka@vscht.cz

In this paper we present results of the mathematical modeling of AC electroosmotic micropumps. Unlike others we use the full dynamic description, instead of the linearized model. Skewed hybrid discretization meshes are employed in order to accurately capture the main features of the studied system. Also, we introduce zig-zag electrode arrangements for traveling-wave electroosmotic micropumps. The detailed analysis of the system behavior is presented by means of the examination of the model properties profiles.

Keywords: multiphysics, microfluidics, multiscale modeling, ac electroosmosis, lab-on-a-chip

1 Introduction

Alternating current electroosmotic micropumps are meant for the use in a variety of portable microfluidic systems such as lab-on-chip devices. Electroosmotic pumps usually operate with water electrolytes. The normal component of an electric field imposed on an array of electrodes attracts oppositely charged particles (counter-ions) from the electrolyte and the electric double layer (EDL) is formed. The polarization means the formation of electric double layers. The component of the electric field parallel to the surface acts on the electric charge stored in the double-layers and, coupled with viscous forces, induces the net fluid flow. This kind of fluid motion is referred as the electroosmotic flow.

AC electroosmotic pumps typically consist of an electrode array with a periodical motif placed on the bottom wall of a microfluidic channel. First experiments proved that the system of two electrodes of the same size powered by AC signals shifted by 180 ° produces flow patterns consisting of four counter-rotating vortices but no net flow [1, 2, 3]. In order to achieve a nonzero net flow velocity, the system symmetry has to be broken [4]. The subsequent force imbalance leads to the desired pumping effect. There are two basic kinds of AC electroosmotic pumps, the asymmetric [5, 6, 7] and the traveling wave [8, 9, 10], both incorporating the principle of broken symmetry.

We focus on the traveling wave pumps which are usually driven by a three of four phase electrical AC signal. The electric signal imposed on adjacent electrodes in the four electrode arrangement is shifted by 90 ° and thus a traveling wave is generated. Such electrode arrays can be represented by four electrodes of equal size separated by narrow gaps. A typical four-phase electroosmotic micropump cannot be constructed in one layer. (with the exception of spiral design [11]). The necessity to separate four electrode arrays into more electrode layers results in much more difficult fabrication.

We introduce the zig-zag arrangement for traveling wave pumps. The zig-zag arrangement can be derived from the standard variant by moving all the even electrodes from the bottom on to the top channel wall. The first electrode is virtually split in half (Fig. 1). We note that the zig-zag design of electrode arrays allows using the interdigital technique [12]. Interdigitated electrodes can be fabricated easily. In addition, electrodes can be extended, which has a positive influence on the flow rate. The electrode extension introduces an electrode overlap that means a part of top (bottom) electrode is above (under) the electrode in the bottom (top) array.

The zig-zag array shows a flow reversal at high frequencies in systems with overlapping electrodes. The reversal transport means the electrolyte flows in the opposite direction than the driving traveling wave.

Figure 1: One periodic segment of the zig-zag traveling wave pump. Light gray and dark gray represent the substrate layers (glass or plexiglass) and the electrodes (gold), respectively. Black lines correspond to solid-electrolyte interfaces.

2 Mathematical Description

2.1 Prerequisites

Due to the periodical character of the system geometry and the driving signal, we assume periodical character of the solution. The modeling domain has been restricted to one periodical segment $\Omega \subset \mathbb{R}^2$ of the length L and height H in the cartesian coordinate system $\mathbf{x} = (x, y)$.

We use the dimensionless coordinate system scaled by the spatial period L: $\tilde{\mathbf{x}} = (\tilde{x}, \tilde{y}) = (x/L, y/L)$.

The system state is described by spatio-temporal fields, the electric potential φ, the electrolyte/salt concentration c, the electric charge density q, the velocity vector $\mathbf{v} = (u, v)$ and the pressure p.

The characteristic values are set to

$$\begin{array}{ll} \lambda_D^2 = \varepsilon RT/(2c_0F^2), & t_0 = \lambda_D L/D, \\ \phi_0 = RT/F, & q_0 = Fc_0, \\ v_0 = D/L, & p_0 = 2c_0RT. \end{array} \quad (1)$$

The parameter λ_D denotes the electric double layer thickness and $t_0 = \tau_c$ represents the characteristic electrode charging time (the double layer relaxation time).

The dimensionless properties are defined as follows:

$$\tilde{\varphi} = \varphi/\phi_0, \quad \tilde{c} = (c^+ + c^-)/(2c_0) - 1, \quad (2)$$

$$\tilde{q} = F(c^+ - c^-)/(2c_0), \quad (3)$$

$$\tilde{\mathbf{v}} = (u/v_0, v/v_0), \quad \tilde{p} = p/p_0. \quad (4)$$

Material properties of an symmetric uni-univalent electrolyte are described by the Rayleigh and Schmidt numbers:

$$\mathrm{Ra} = \frac{\varepsilon}{\eta D}\left(\frac{RT}{F}\right)^2, \quad \mathrm{Sc} = \frac{\eta}{\rho D} \quad (5)$$

2.2 Governing equations

The system behavior is governed by the Gauss law of electrostatics in the form of the Poisson equation (6), the local balances of the ionic species (7) and the electric charge (8), the Navier-Stokes (9) and the continuity equation (10):

$$0 = -\tilde{\nabla}^2\tilde{\varphi} - \tilde{q}/\lambda_D^2 \quad (6)$$

$$\frac{1}{\tilde{\lambda}_D}\frac{\partial \tilde{c}}{\partial \tilde{t}} = -\tilde{\nabla}\cdot\tilde{\mathbf{J}} \quad (7)$$

$$\tilde{\mathbf{J}} = \tilde{\mathbf{v}}\tilde{c} - \tilde{\nabla}c - \tilde{q}\tilde{\nabla}\tilde{\varphi}$$

$$\frac{1}{\tilde{\lambda}_D}\frac{\partial \tilde{q}}{\partial \tilde{t}} = -\tilde{\nabla}\cdot\tilde{\mathbf{I}} - \frac{\tilde{q}}{\tilde{\lambda}_D^2} \quad (8)$$

$$\tilde{\mathbf{I}} = \tilde{\mathbf{v}}\tilde{q} - \tilde{\nabla}q - \tilde{c}\tilde{\nabla}\tilde{\varphi}$$

$$\frac{1}{\tilde{\lambda}_D \mathrm{Sc}}\frac{\partial \tilde{\mathbf{v}}}{\partial \tilde{t}} = -\tilde{\nabla}\tilde{p} - \tilde{\nabla}\cdot\mathbb{T} - \frac{\mathrm{Ra}}{\tilde{\lambda}_D^2}\tilde{q}\tilde{\nabla}\tilde{\varphi} \quad (9)$$

$$\mathbb{T} = \left[\frac{\tilde{\mathbf{v}}\tilde{\mathbf{v}}}{\mathrm{Sc}} - \tilde{\nabla}\tilde{\mathbf{v}}\right]$$

$$0 = -\tilde{\nabla}\cdot\tilde{\mathbf{v}} \quad (10)$$

$\tilde{\mathbf{J}}$ and $\tilde{\mathbf{I}}$ stand for the ionic species flux density and the electric current density, respectively.

2.3 Initial and boundary conditions

For shortness, we introduce a symbolism for system boundaries. The entire solid-electrolyte interface is represented by a set $\tilde{\mathbb{B}} = \tilde{\mathbb{B}}_e \bigcup \tilde{\mathbb{B}}_d = \tilde{\mathbb{B}}_b \bigcup \tilde{\mathbb{B}}_t$. Here, $\tilde{\mathbb{B}}_d$ represents all dielectric-electrolyte interfaces and $\tilde{\mathbb{B}}_e = \sum_{m=0}^{4} \tilde{\mathbb{B}}_{e,m}$ represents the sum of the m-th electrode-electrolyte interfaces, where m is the electrode sequential number. Subscripts $_b$ and $_t$ refer to the top and the bottom channel wall, respectively.

Now we can describe conditions at the phase interfaces as follows:

$$\tilde{\varphi} = \tilde{\varphi}_{\mathrm{m}}, \quad \tilde{\mathbf{x}} \in \tilde{\mathbb{B}}_{\mathrm{m}}, \quad (11)$$

$$\mathbf{n}\cdot\tilde{\nabla}\tilde{\varphi} = 0, \quad \tilde{\mathbf{x}} \in \tilde{\mathbb{B}}_{\mathrm{d}}, \quad (12)$$

$$\tilde{\mathbf{v}} = 0, \quad \mathbf{n}\cdot\tilde{\mathbf{J}}^{\pm} = 0, \quad \tilde{\mathbf{x}} \in \tilde{\mathbb{B}}. \quad (13)$$

The left and the right boundary of the modeling domain are periodically coupled:

$$\begin{array}{rl} \tilde{\xi}(\tilde{x} = 0, \tilde{y}, \tilde{t}) = & \tilde{\xi}(\tilde{x} = 1, \tilde{y}, \tilde{t}), \\ \tilde{\xi} = & \{\tilde{\varphi}, \tilde{c}^{\pm}, \tilde{\mathbf{v}}, \tilde{p}\}. \end{array} \quad (14)$$

In order to get the hydrodynamically consistent set of boundary conditions we have to

fix a reference value of the pressure in one arbitrary point:

$$\tilde{p} = 0, \quad \tilde{\mathbf{x}} = (0, 0). \tag{15}$$

3 Methods

The numerical analysis of the model has been performed in Matlab 2007/COMSOL Multiphysics 3.4 package. Scripts combining functions of both Matlab and COMSOL are used for handling our specific requirements.

First, the periodic character of the modeled system makes possibility to extract the minimal common part–the periodic segment. The behavior of the entire system may be represented by this unit.

Second, the periodical segment is subdivided into the electrolyte bulk domain and narrow regions above the electrodes in order to provide the opportunity for the detailed study of the electric double layer dynamics.

Third, the most rapid and significant changes of system properties take place in electric double layers regions, especially in immediate proximity of electrode corners. A discretization mesh has to be sufficiently dense in these critical regions and cover the entire periodical segment at the same time. The size ratio of the periodic element and the double layer thickness is quantified by the parameter $\tilde{\lambda}_D = \lambda_D/L$. In order to capture the double layer dynamics, the size of the mesh elements has to be even smaller in the double layer regions. Ultimately, the ratio of sizes of the largest triangular and the smallest quadrilateral element might exceed value of 10^3.

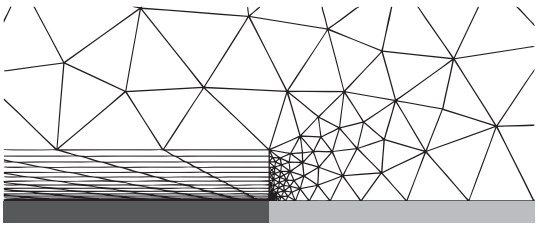

Figure 2: The skewed hybrid discretization mesh detail.

Hybrid discretization meshes consisting of the triangular part in the electrolyte bulk region and rectangular parts for the double layer regions has been employed in our previous simulations.

With regard to the driving mechanism of the electroosmotic flow, skewed quadrilaterals have been used in the double layer caps. The electric field generated by the electrodes has rather a radial character at the critical zones. Rectangular discretization meshes can resemble to this trend by an element densification towards the electrode corners. This densification has a negative impact to the element count and causes unwanted element crowding in the electrolyte bulk region. The skewed quadrilaterals (Fig. 2) can introduce a better numerical approximation without the element crowding effect. By default, COMSOL distributes mesh elements isotropically. In addition, the element growth specification by a vector is allowed. In the double layer regions, the elements grow exponentially in the direction perpendicular to the electrode surface. The similar exponential elements size growth is introduced at the electrode edges and between the corners, while on the opposite cap edge (further in the electrolyte) the equidistant character is preserved.

4 Discussion

Zig-zag arrangements display flow reversals. For sufficiently wide electrodes ($\tilde{L}_e > 1/4$), the flow direction is reversed at high frequencies (Fig. 3). For electrodes narrower than $L/4$, the flow reversal does not occur at all. The zig-zag traveling wave pump can be decomposed into the system of two-electrode arrays, in which the upper array is shifted in x-direction by $L/4$. As mentioned above, the two-electrode symmetric system produces no net flow. The force imbalance is introduced by shift of the upper array. Moreover, the arrays can interact over the channel. The intensity of this interaction depends on the channel height, the ac signal frequency, the electrolyte concentration and the AC signal amplitude.

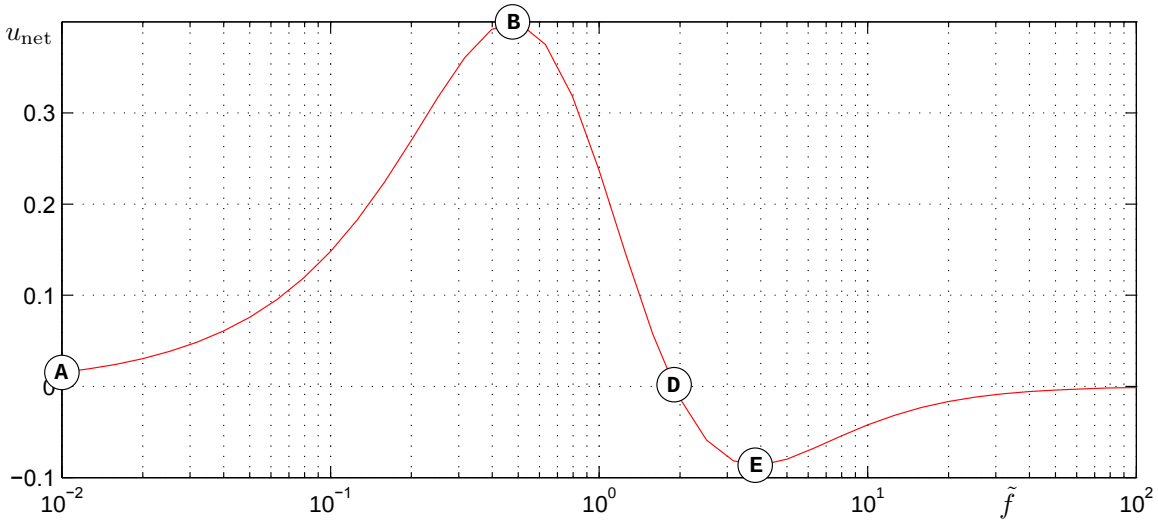

Figure 3: The dependence of the dimensionless net velocity on the dimensionless frequency. $H = 0.2\,L$, $L_e = 0.45\,L$, and $\tilde{\lambda}_D = 0.001$.

The predicted flow reversal might be a consequence of the electrode array interaction at high frequencies.

The double layer thickness is in this case one thousand times smaller than the system length, $\tilde{\lambda}_D$=0.001, hence, the most significant changes of the system properties take place in very narrow regions.

4.1 Forward flow regime

At very low frequencies (Fig. 3, marker **A**), the zig-zag pump behaves like a pair of symmetric two-electrode arrays, since the interactions between arrays are strongly suppressed by the electrode polarization.

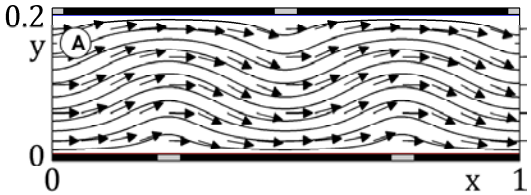

Figure 4: The velocity vector field at low frequencies, $\tilde{f} = 0.01$.

Vortices, usually incidental with the electroosmotic flow, are not apparent at these conditions (Fig. 4).

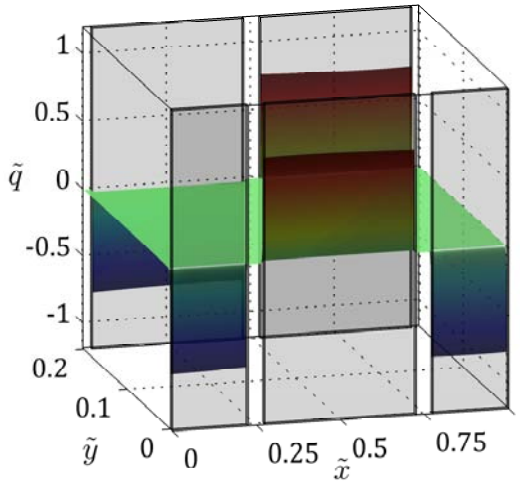

Figure 5: The electric charge density field at low frequency $\tilde{f} = 0.01$. Gray transparent boxes represent electrodes.

Generally speaking, the highest magnitude of the electric charge density is localized at the electrode corners. Beyond the narrow zone of the electric double layers, the field strength has a constant value equal to zero (the electrolyte bulk is shielded by the double layers from the external electric field). Changes in the electrode potential are sufficiently slow to allow the complete electrode shielding/polarization at low frequencies. Such a situation is depicted in Fig. 5 There is enough time for the transport of oppositely charged ions (counter-ions) from the electrolyte bulk into the double layers.

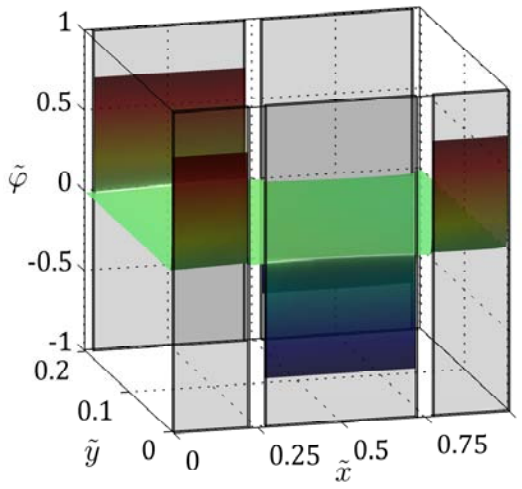

Figure 6: The electric potential field at low frequency $\tilde{f} = 0.01$. There is apparent the external electric field shielding.

The electric field generated by the charge stored in the double layers shields the electrolyte bulk from the external field (Fig. 6).

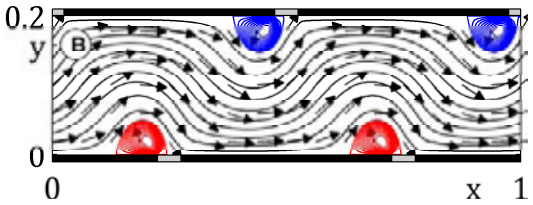

Figure 7: The velocity vector field in forward regime at optimal frequency, $\tilde{f} = 0.326$.

The net velocity of AC electroosmotic pumps typically reaches its maximum at the optimal frequency $f_0 = D/(\lambda_D L)$, which is the reciprocal value of the electric double layer relaxation time $\tau_c = \lambda_D L/D$. In the case of zigzag traveling wave pumps, the maximal net velocity occurs also close to $\tilde{f}_0$. The figure 7 shows the flow patterns at the optimal frequency (cf. Fig 3, marker **B**).

The electric charge density q and the electric potential φ fields, respectively, are depicted in Fig. 8 and Fig. 9, respectively, for entire modeling domain.

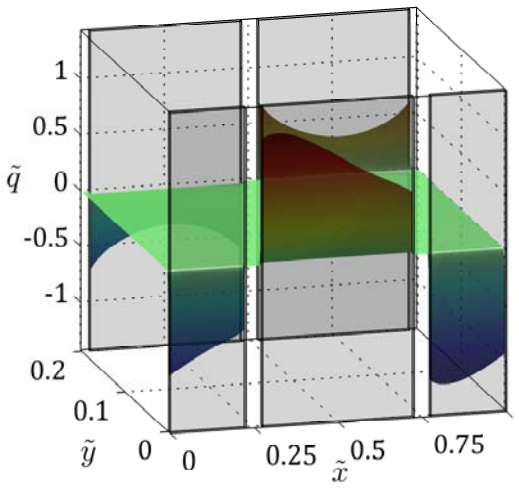

Figure 8: The electric charge density field at optimal frequency $\tilde{f} = 0.326$.

Typically, the electric charge density field values change first at electrode edges, then follows the rest in between. The symmetry of the profile is (sort of) broken, which is caused by the interactions of the electrodes in the opposing electrode array. In figure 8, the broken symmetry is apparent and the wave maximum is shifted to the left corner.

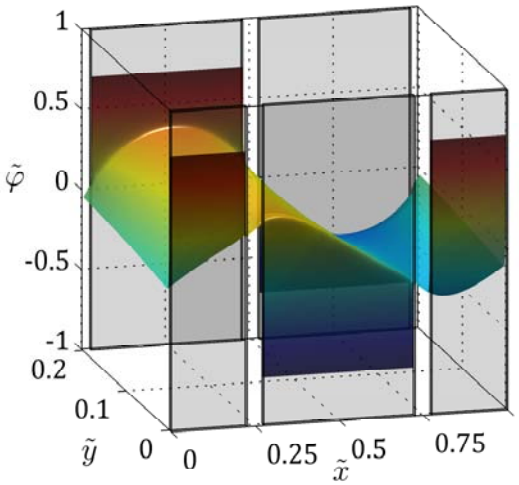

Figure 9: The electric potential field at optimal frequency $\tilde{f} = 0.326$.

With growing frequency, the electrode polarization weakens due to the incomplete charging and the electrolyte bulk is also affected by the driving field.

4.2 Regime at the point of reversion

Examinations of the velocity vector field dynamics reveals a gradual growth of the fluid vortices with increasing frequency (Fig. 3 markers **B**–**D**). There is a noticeable tendency of the vortices to interconnect adjacent electrode corners across the channel.

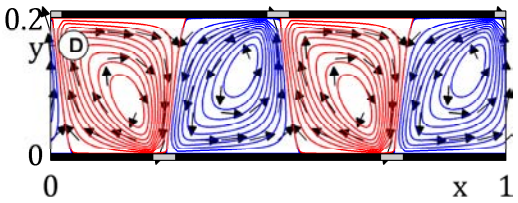

Figure 10: The velocity vector field at the point of reversion $\tilde{f} = 2$.

As soon as the vortices reach the nearest corners, the net flow velocity tends to change its direction (Fig. 10).

4.3 Reversed flow regime

The flow reversal has been observed in many experiments performed with typical AC electroosmotic micropumps, which have electrode arrays only at one channel wall. There is no consistent underlaying theory explaining this phenomenon yet. In the case of the zig-zag geometry, the flow reversal may be caused by the competition between two opposing electrode arrays.

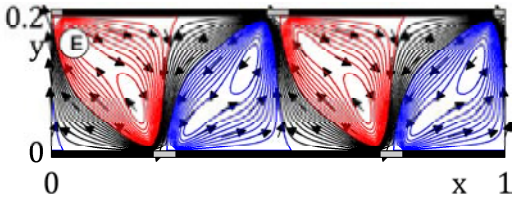

Figure 11: The velocity vector field in the reversed regime $\tilde{f} = 4$.

Further increasing of the ac signal frequency deforms the shape of the fluid vortices (Fig. 11). Eventually, the vortices split-up and disappear while the net velocity tends from its minimum to zero.

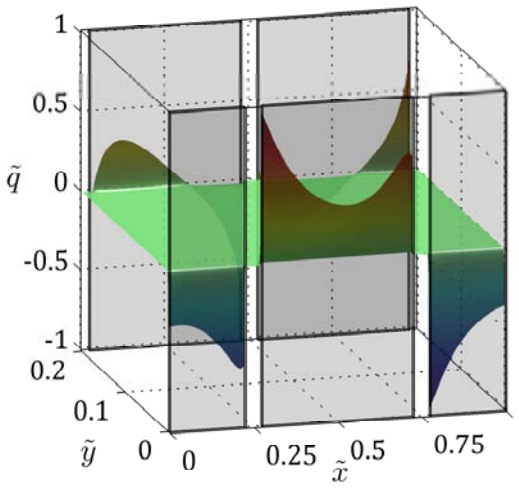

Figure 12: The electric charge density field at high frequency $\tilde{f} = 10$.

In some cases, the electric charge density changes its sign even along a single electrode (see Fig. 12).

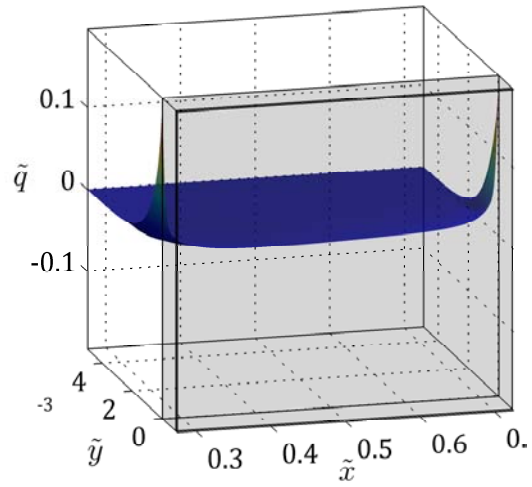

Figure 13: The electric charge density field at at very high frequency $\tilde{f} = 100$ above the central bottom electrode.

The subdivision of the modeling domain (cf. Fig. 13) allows a detailed inspection of the model properties separately. In the reversed flow regime, the electric charge density field is deformed. Electric double layers have not enough time to fully charge and only counter-ions in a close proximity of the electrode corners can respond to rapid electric field changes.

At high frequencies, there is not enough time for complete double layer charging and

the electric field can expand over the channel (Fig. 14).

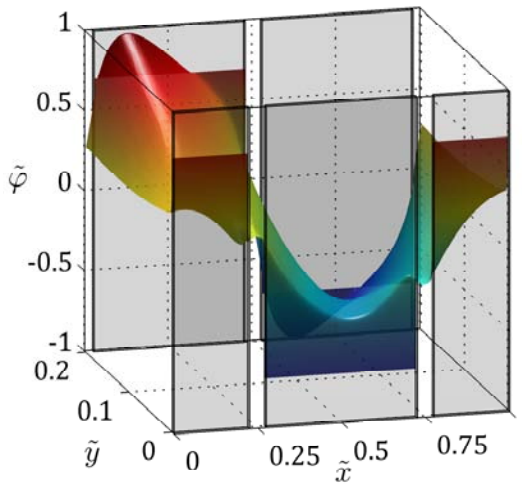

Figure 14: The electric potential field at high frequency $\tilde{f} = 4$.

At frequencies more than 100 times higher than the characteristic one, the deformations of the charge density field weakens and eventually cease.

5 Conclusions

The innovative zig-zag arrangement for traveling wave electroosmotic micropumps was introduced. The zig-zag pumps are easier to construct than classical traveling wave pumps and display the flow reversal as a general feature caused by electrode overlaps.

The skewed hybrid mesh was used for the modeling domain discretization. The hybrid meshes are necessary for modeling systems with thin boundary layers.

COMSOL Multiphysics together with Matlab makes possible a detailed analysis of the system properties profiles in order to understand the studied system behavior.

References

[1] N.G. Green, A. Ramos, A. González, H. Morgan, and A. Castellanos, Physical review E **61** (2000), 4011–4018.

[2] A. González, A. Ramos, N.G. Green, A. Castellanos, and H. Morgan, Physical review E **63** (2000), 4019–4028.

[3] N.G. Green, A. Ramos, A. González, H. Morgan, and A. Castellanos, Physical review E **66** (2002), 026305.

[4] A. Ajdari, Physical Review E **61** (2000), R45.

[5] V. Studer, A Pépin, Y. Chen, and A. Ajdari, Microelectronic Engineering **61-62** (2002), 915–920.

[6] M. Mpholo, C.G. Smith, and A.B.D. Brown, Physical review E **63** (2000), 016305.

[7] L.H. Olesen, H. Bruus, and A. Ajdari, Physical Review E **73** (2006), 056313.

[8] A. Ramos, H. Morgan, N.G. Green, A. González, and A. Castellanos, Journal of Applied Physics **97** (2005), 084906.

[9] P. García-Sánchez, A. Ramos, N.G. Green, and H. Morgan, Journal of Physics: Conference series **142** (2008), 012055.

[10] A. González, A. Ramos, and A. Castellanos, Microfluid Nanofluid **5** (2008), 507–515.

[11] B.P. Cahill, L.J. Heyderman, J Gobrecht, and A. Stemmer, Physical review E **70** (2004), 036305.

[12] A.B.D. Brown, C.G. Smith, and A.R. Rennie, Physical review E **63** (2000), 016305.